



Adsorption of Zirconium using Hyper Cross Linkage Phospho-thiol Polymer and Application of its Separation from Rosetta Zircon Mineral Concentrate

M. Demerdash*

Nuclear Material Authority, Madii, Cairo, Egypt



Abstract

Hyper cross linkage phosphothiol polymer (HCPTP) is a new adsorbent that offers an excellent synergistic effect for the adsorption of Zirconium ions. FT-IR, ¹H NMR, ¹³C, and ³¹P NMR, FTIR, SEM, GC-Mass, and BET were used to characterize the modified new chitosan adsorbent. The Freundlich isotherm model accurately represents the adsorption effect with a maximum adsorption capacity of 307 mg/g. It was noted that the up-taking process of Zirconium ions corresponded more closely to the pseudo-second order kinetic. The thermodynamic tools ΔS , ΔH and ΔG were also evaluated indicating spontaneous endothermic adsorption process with a randomness increasing. The prepared new adsorbent is successfully used to adsorption of Zirconium ions from the actual leach liquor of Egyptian Rosetta zircon sample.

Keywords: Zirconium; Adsorption; Separation; Hyper cross linkage polymer; phosphothiol polymer

1- INTRODUCTION

Hyper-cross-linked porous polymers (HCP) are a series of porous organic polymers and have highly knitted cross-linking network structures. A large number of pores are produced by knitting rigid aromatic building blocks with external crosslinkers [1-3]. A Friedel-Crafts reaction is a type of organic coupling reaction that uses an electrophilic aromatic substitution to attach substituents to aromatic rings. The resulting polymers consist of aromatic rings joined together through aliphatic bridges. It is a basic and benign reaction that's been frequently employed to make low-cost, high-surface-area microporous polymers [4-5]. HCP have been developed in the past for a variety of applications, including sorption [6], gas separation [7] and water pollution control [8]. The HCP adsorbents have several distinct physicochemical characteristics [9]. One of the most significant advantages of this material is that it requires low-cost monomers, reaction medium, and catalysts, and the reaction conditions are simple to handle and regulate, resulting in high yield products [10-11]. The monomer with a three-dimensional extended structure is beneficial to create porous HCP with a large surface area. The history of crosslinked polystyrene networks can be traced back to the 1930s, [12] and after many years of research and development, they are still widely used in adsorption

and separation. In the 1970s, Davankov et al. first introduced HCPs, which possess more extensive crosslinks than conventional crosslinked polystyrene. [13] The formation of a high level of crosslinks leads to nanoporous structures, and the rigid networks prevent the nanoporous structure from collapse. Compared to traditional divinylbenzene crosslinked polystyrene, HCPs exhibit permanent small pores, high surface areas, and large micropore volumes. [14]

Zirconium is used in nuclear reactor technology in the form of zircalloys as cladding material for the uranium fuel and for other reactor internals. Due to ageing effect of reactor vessels, erosion starts and leads to contamination of the coolant water with radioactive species of zirconium, thus posing hazards to the systems and environment. Zirconium and its compounds are also extensively used in chemical industries, steel and cast manufacturing, surface agent on satellites, lamp filaments, welding fluxes, in vacuum tubes, preparation of water repellent textiles, dyes pigments, ceramics, glass and abrasives. It is, therefore, important to decontaminate the reactor coolant water from radioactive zirconium and from other industrial effluents, before their safe disposal into water bodies [15, 16].

Zr(IV) is one of the abundant and widely distributed elements on Earth's crust. Most of the Zr compounds are used in the ceramic industry, refractory, glazes, enamels and abrasive grits and compounds for

*Corresponding author e-mail: doctormohameddemerdash@yahoo.com; (Mohamed Demerdash)

Receive Date: 31 July 2022, Revise Date: 19 August 2022, Accept Date: 28 August 2022.

<https://doi.org/10.21608/ejchem.2022.153460.6646>

©2023 National Information and Documentation Center (NIDOC)

electrical ceramics. Zr metal is also used for cladding uranium fuel elements for nuclear power plants. The industrially important Zr minerals are baddelyite (ZrO_2) and zircon ($ZrSiO_4$) [17]. Zirconium is significant engineering material for nuclear energy application due to its high transparency to neutrons.

Recently, with the increasing demands for the productions of high grade zirconium, hafnium and their compounds, methods and high selective extractants for the separation of them have become very important. Traditional methods such as fractional crystallization, fractional precipitation, ion exchange, solvent extraction, molten salt distillation and selective reduction are often used [18]. And extractants such as methyl isobutyl ketone (MIBK), N235 and TBP are applied into solvent extraction, but in light of their disadvantages of great treatment capacities, high efficiency and environmental pollutions, industrializations are restricted [19]. The demand for development of high efficient methods of using highly specific ion recognition extractant to separate zirconium from hafnium is needed urgently.

Zirconium is a suitable metal for cladding nuclear fuel and controlling materials in nuclear reactors, space, metal alloys, piping, etc.; because it takes advantage of its excellent properties such as thermal stability, mechanical strength and highly resistant to corrosion by alkalis, acids, salt water and other agents [20]. Therefore, separation and recovery of even trace amounts of them from waste water can be worthwhile. Several methods such as ion exchange, solvent extraction and precipitation for the removal of this metallic ion from aqueous solution have been investigated [21–25].

The aim of this work was directed for the preparation and characterization of a new high cross linkage polymer capable of adsorption of Zr(IV) with high efficiency. The uptake behavior as of the adsorbent toward Zr(IV) was investigated. The sorption data obtained were treated according to the Langmuir and Freundlich adsorption isotherm. Kinetic and thermodynamic parameters of adsorption reaction were calculated. And finally, the application on separation of Zr(VI) from rosetta zircon mineral concentrate.

1. EXPERIMENTAL

2.1. CHEMICALS

Bisphenol A, (2,2-Bis(4-hydroxyphenyl)propane, 4,4'-Isopropylidenediphenol), $AlCl_3$ (anhydrous), $FeCl_3$ (anhydrous), Formaldehyde dimethyl acetal (FDA), 1,2-dichloroethane (DCE), and zirconium oxychloride ($ZrOCl_2 \cdot 8H_2O$) were purchased from Fluka, Phosphorus oxychloride, Methanol, and

Carbon disulfide were purchased from Aldrich (Germany), All other chemicals were ADWIC products (Egypt).

2.2. Preparation of Zirconium solution:

The stock zirconium solution was prepared by dissolving 3.53 g of zirconyl oxychloride in 100 mL of ultra pure water and then, diluted to required working concentrations in ultra pure water.

2.3. Preparation of Hyper crosslinkage polymer using bisphenol A.

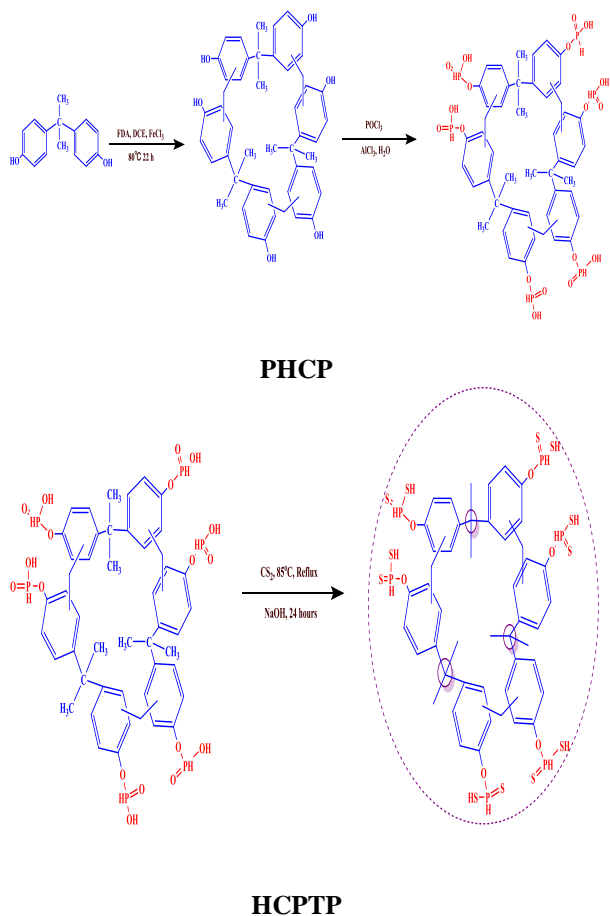
Bisphenol A (2,2-Bis(4-hydroxyphenyl)propane, 4,4'-Isopropylidenediphenol) (20mmol) was dissolved in anhydrous 1,2-dichloroethane, cross-linker Formaldehyde dimethyl acetal (FDA:60mmol) and the catalyst (anhydrous $FeCl_3$:60mmol) were added in it under nitrogen. The mixtures were stirred at room temperature firstly then were stirred at 40°C for 6 h followed by 80°C 22 h to react completely. The precipitate was boiled in methanol at 50°C for 30 h, then washed with methanol until the filtrate became clear and finally dried in vacuum at 60 °C for 24 h. the produced product was named **HCP**

The synthetic way of **HPCP** was shown in Fig. 1. The phosphorylation process was carried out by mixing of 1 g synthetic HCP, 0.15 g $AlCl_3$ (anhydrous) with 20 mL phosphorus oxychloride for 30 h at the temperature of 115 °C. Install tail gas absorber to absorb HCl in the reaction process. Then in an ice bath, 200 mL distilled water was added to the resulting mixture slowly drop by drop.

The mixture was filtered and washed with distilled water several times and dried in vacuum at 80 °C for 30 h.

2.4. Reaction of the phosphorylated with carbon disulfide (CS_2)

The phosphorylated HCP (0.5 g), NaOH 1 M in ethanol (30 mL) and CS_2 (1.6 mL) were placed in a reactor (100 mL) equipped with mechanical stirring. The reaction was maintained at room temperature for 6 days, the produced product is called as **HCPTP (Hyper crosslinkage phosphothiol polymer)**



Scheme 1. Preparation of hyper crosslinkage polymer (HCP), Phosphorylated hyper crosslinkage polymer (PHCP), Phosphothiol polymer, and hyper crosslinkage phosphothiol polymer (HCPTP).

INSTRUMENTATION

Shimadzu UV–Visible Recording Spectrophotometer (UV-160A) manufactured and supplied by Shimadzu Kyoto, Japan was used for estimation of Zr(IV) and Mo(VI) concentration. The adsorbent was characterized with respect to its pore structure and surface area using nitrogen adsorption/desorption at 77 K which was conducted using a gas sorption analyzer (Quantachrome, NOVA 1000e series, USA), FTIR spectrum of the charcoal sample was recorded using a Nicolet spectrometer from Meslo, USA to identify the functional groups. Simultaneous differential thermal and thermogravimetric analyses (DTA/TGA) of activated carbon were carried out using DTA and TGA with sample holder made of platinum using a Shimadzu DTG-60/60H thermal analyzer, Japan. It was used for the measurements of the phase changes and weight losses of the sample at heating rate of 10 °C/min in presence of nitrogen gas to avoid thermal oxidation of the adsorbent sample. The sample was

heated in a platinum crucible from room temperature to 1000 °C.

BATCH ADSORPTION STUDIES

The process variables i.e., pH (0.5–4) Zr(IV) ions initial concentration (10–100 mg/L), adsorbent dose (0.05–0.25 mg/L), contact time (10–180 min), temperature (30–70 °C), were investigated. NaOH and HCl 0.1 N solutions were used for pH adjustment. For adsorption experiments, the respective amount of adsorbent was mixed with 20 mL of Zr(IV) solution placed on a rotating shaker (PA 250/25H) with constant shaking. After stipulated time, the contents were filtered to separate solution from adsorbent. The xylenol orange was used for the spectrophotometric determination of Zr(IV) ions at 535 nm and the adsorption capacity (q_e) was determined using relation shown in Eq. (1).

$$Q_e = \frac{(C_o - C_e)V}{W} \dots\dots\dots(1)$$

Where Q_e (mg/g) is an adsorption capacity, C_o (mg/L) is an initial concentration, C_e (mg/L) is the final concentration after adsorption, W is the added adsorbent weight (g), and V is the batch solution volume (L).

Batch studies were performed by using a calculated amount of adsorbent in 250 mL flasks at 25°C under continuous agitation at 150 rpm in a rotary shaker. The adsorbents were withdrawn at fixed margins of time, and concentration of Zirconium ions in the solution was determined. Small portions of the solution were collected for measurements with minimum disturbance to the adsorption system by keeping the final volume of the solution unchanged. The adsorption capacity of the samples was calculated by measuring the Zirconium concentration at a fixed interval time.

DESORPTION EXPERIMENTS

Desorption is an extremely crucial rule, as both adsorbent regeneration and the Zr(IV) ions recovery are being greatly demanded in the adsorption experiments. Desorption examinations were done in the batch system using the loaded adsorbent immediately after the adsorption experiment. Herein, different concentration of HNO₃, EDTA and HCl were used as desorption agents, desorption time and temperature were studied. The concentration of metal ions in the supernatant has been spectrophotometrically performed using xylenol orange as indicator.

RESULTS AND DISCUSSIONS

CHARACTERIZATIONS OF HCPSP

SEM of PHCP and HCPSP:

The surface morphology of the prepared adsorbent was characterized by SEM, as shown in Fig. 1. Before reaction with carbon disulfide PHCP and after reaction HCPSP, the resin surface was more uniform and smooth. While for HCPSP, the adsorbent showed more roughness and undulations.

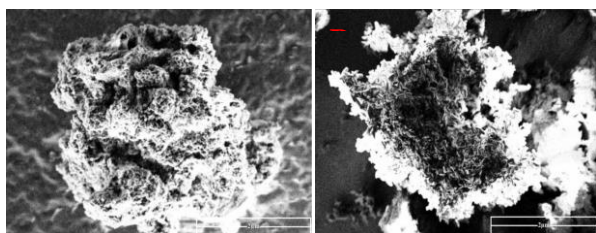


Fig. (1): SEM of (A) PHCP and (B) HCPTP

FTIR of PHCP and HCPTP:

FT-IR was used to better understand the specific compositions of the produced materials, and the results are shown in Fig. 2. In the complete spectra, the peaks of 1637 cm^{-1} and 1470 cm^{-1} are in connection with aromatic ring vibrations. The broad peak band at 3441 cm^{-1} is due to the $-\text{OH}$ bond's vibration. Majority polymers revealed an intense water sorption peak at $\sim 3400\text{ cm}^{-1}$ due to physisorbed water [26].

In HCP, the band at 1109 cm^{-1} is due to C–O group, and disappearance of the peak in PHCP which indicates that the phenolic hydroxyl group is converted to C–O–P, which proves that the graft phosphorylation process is successful. [27, 28]

After the phosphorylation reaction, the chemical structure of the phosphorylated HCP was confirmed by its FTIR bands related to the P–H stretching vibration (2350 cm^{-1}), P=O stretching vibration (1170 cm^{-1}) and P–OH stretching vibration (991 cm^{-1}) and The peak observed at 874 cm^{-1} is related to the P–O–C bending vibration [29] (Fig. 2b). None of these were observed in the spectrum of the HCP. The conversion of phosphoryl groups into sulfophosphoryl ones was confirmed by the presence of three bands (at 2540 , 2349 and 651 cm^{-1}), attributed to the S–H stretching vibration, P–H stretching vibration and P=S vibration (Fig. 2c), respectively. The reaction with CS_2 is typically a difficult reaction, leaving therefore to a low conversion degree [30–32].

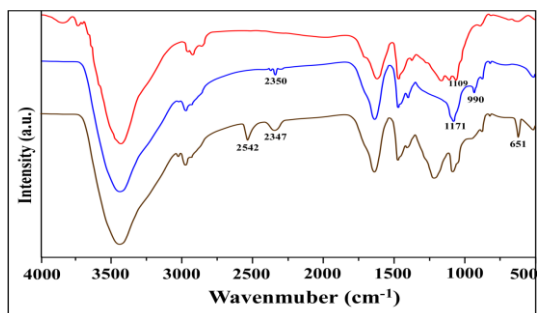


Fig. (2): FTIR spectra of the HCP, PHCP, and HCPTP.

Brunauer–Emmett–Teller (BET) Surface Area Analysis

The materials were further characterized by BET analysis (Fig. 3). The N_2 adsorption-desorption curves of the PHCP are shown in Fig. 3 (a). We can see that the nitrogen sorption isotherm as if approximate

to the type-I category [33] and mesopores are existence because of an obvious hysteresis loop in the desorption isotherm. As shown in Table 1, the BET surface area of PHCSP is $693\text{ m}^2/\text{g}$, which is larger than PHCP ($279\text{ m}^2/\text{g}$). This is due to the Cardo structure of bisphenol-A. On comparison with HCP, the BET surface area and pore volume for PHCP decreased from $482\text{ m}^2\cdot\text{g}^{-1}$ and $0.29\text{ cm}^3\cdot\text{g}^{-1}$ to $279\text{ m}^2\cdot\text{g}^{-1}$ and $0.14\text{ cm}^3\cdot\text{g}^{-1}$. These results were thought to be due to the large number of phosphate groups occupying the pore space in the PHCP. the BET surface and pore volume of PHCP after modification, increased than the phosphated one which is beneficial for Zr(IV) adsorption. As shown in Fig. 3 (the insets a and b),

Table (1). Surface area and pore size of HCP, PHCP, and HCPTH

Sample	BET surface area (m^2/g)	Total pore volume (cm^3/g)	Average pore diameter (nm)
HCP	482	0.29	2.7
PHCP	279	0.14	2.91
HCPTP	693	0.35	2.28

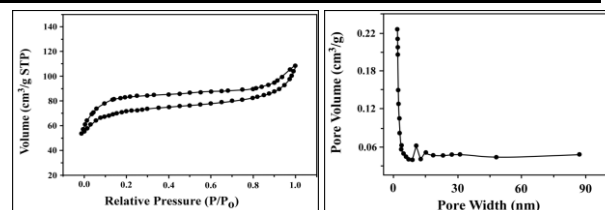


Fig. (3).A. N_2 sorption isotherms of (a) PHCP and (b) Pore volume.

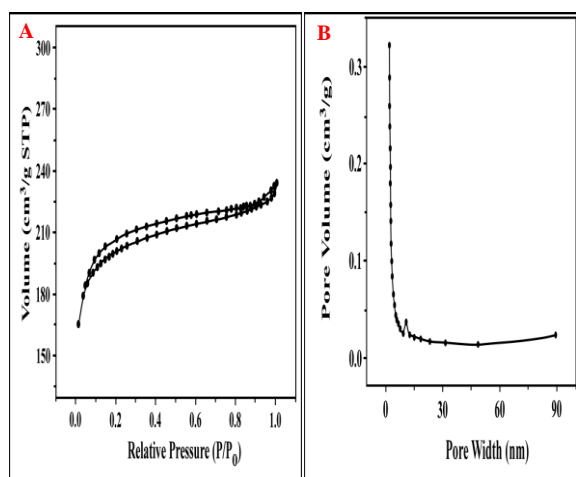
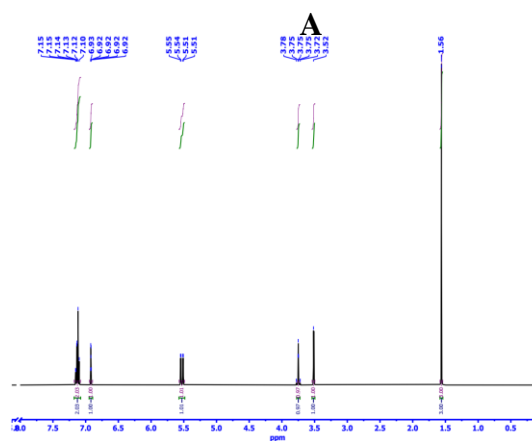


Fig. (3). B. N₂ sorption isotherms of (a) HCPSP and (b) Pore volume.

¹H-NMR analysis.

¹H-NMR (400.15 MHz, DMSO-d₆, 25 °C, TMS) δ, ppm: 1.56 (s, 3H, 6CH₃), 3.52 (s, 1H, 6SH), 5.53 (m, 1H, J=14.3 Hz, 6PH), 6.92 (m, 1H, J=1.9 Hz, 6CH of benzene ring), 7.12 (m, 2H, 12CH of benzene ring). ¹H-NMR analysis with energy of 400.15 MHz and DMSO-d₆ as a diluent is an effective and helpful tool which gives significant data about protons in the synthesized ligand which assist in the structure prediction. The main δ (ppm) assignments appear at 6.92 and 7.12 ppm which are related to -CH protons of benzene ring. The presence of two assignments to -CH of benzene rings is thought to depend on the degree of orientation, proximity and distance from the main active sites which cause difference in the values of the chemical shift and coupling constant. It was observed that the assignment of -SH proton (δ=3.52 ppm) is more de-shielded because of the presence of -P=S (thio-phosphine group), however the normal value is observed nearly between δ=1.5-2 ppm. The proton assignment of -PH group was characterized at a chemical shift of 5.53 ppm. Characterization of bis-phenol chelating ligand using ¹H-NMR is illustrated in Figure 4.



B

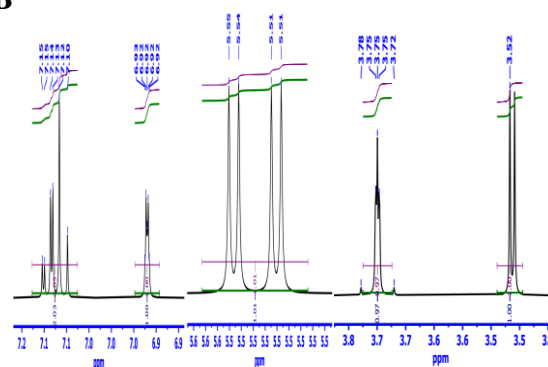


Fig. (4): (A) ¹H-NMR analysis of hyper cross linkage phosphothiol polymer HCPTP. (B). Clarification of ¹H-NMR analysis of hyper cross linkage phosphothiol polymer HCPTP

¹³C-NMR analysis.

¹³C-NMR (125.76 MHz, DMSO-d₆, 25 °C, TMS) δ, ppm: 31.01 (s, J=13 Hz, 6CH₃), 31.28 (s, J=13 Hz, 3CH₂), 42.04 (s, J=5 Hz, 3C), 115.25-153.57 (s, J= 2-7 Hz, carbon of benzene ring). ¹³C-NMR analysis with energy of 125.76 MHz and DMSO-d₆ as a diluent is an effective tool which gives significant data about number of carbon atoms in the synthesized ligand. The main δ (ppm) appeared around 31.01-31.28 ppm which is related to methyl and methylene group respectively. The -CH₃ carbon assignment was found to appear at 14.126 ppm which is more shielded than the other -CH₂ carbons. The deprotonated carbon assignment was found to be more de-shielded than methyl and methylene groups which appears at 42.04 ppm. The higher de-shielded protons of benzene ring was also observed at a high chemical shift between 115.25-153.57 ppm. Specification of bis-phenol chelating ligand using ¹³C-NMR is illustrated in Figure 5.

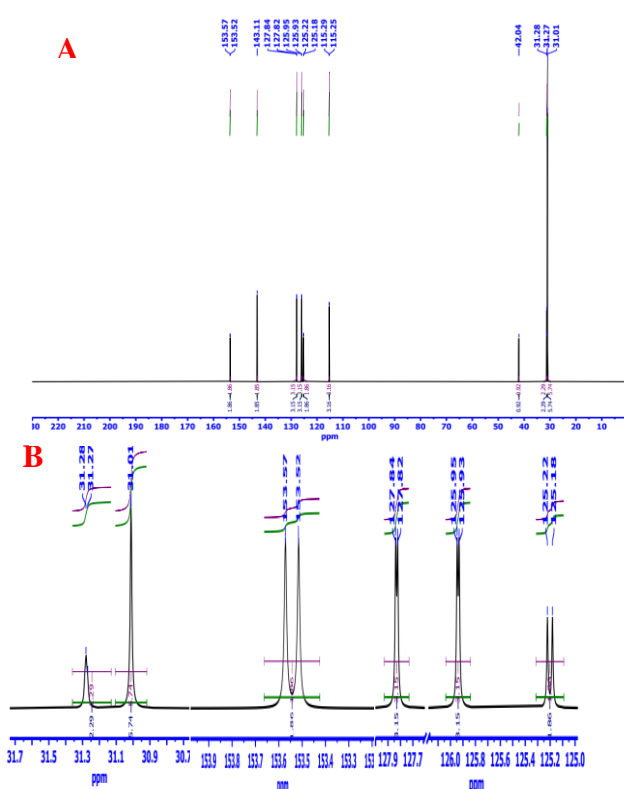


Fig. (5): (A) ^{13}C -NMR analysis of hyper cross linkage phosphothiol polymer HCPTP, (B) Clarification of ^1H -NMR analysis of hyper cross linkage phosphothiol polymer HCPTP.

GC-MS analysis

GC-MS (EI,70 eV), m/z (% rel): $[m/z]^+$ of 78, 120, 34, 94, 105, 93, 190, 43, 91, 107, 178, 128, 142, 30, 156. Anal. Calc. for $\text{C}_{48}\text{H}_{54}\text{O}_6\text{P}_6\text{S}_{12}$ (1297.52 g/mol): C, 44.43; H, 4.2; O, 7.4; P, 14.32; S, 29.65. Found: C, 44.02; H, 4.04; O, 7.22; P, 14.12; S, 29.69. Gas chromatography with Mass spectrometer unit (GC-MS), also considered as an influential and powerful tool for the prediction of the molecular formula, purity and the more stable fragment $[m/z]^+$. The molecular ion peak which represents the molecular weight of the synthesized ligand does not appear in the fragmentation pattern. This disappearance may be due to the high energy used in the electrical impact technique (EI-MS), which categorized as a hard ionization technique causing an extensive fragmentation. Some important fragmentation patterns, which are related to the synthesized bis-phenol, were observed such as $[\text{C}_6\text{H}_6]^+$ with a molecular weight of 78 (benzene ring), $[\text{C}_9\text{H}_{12}]^+$ with a molecular weight of 120 (iso-propyl benzene), $[\text{H}_2\text{S}]^+$ with a molecular weight of 34, $[\text{C}_6\text{H}_6\text{O}]^+$ with a molecular weight of 94 (phenol), $[\text{C}_6\text{H}_5\text{O}]^+$ with a molecular weight of 93 (phenoxide),

$[\text{C}_3\text{H}_7]^+$ with a molecular weight of 43 (propyl carbonium ion), $[\text{C}_7\text{H}_8]^+$ with a molecular weight of 91 (tropilium cation), $[\text{C}_{14}\text{H}_{10}]^+$ with a molecular weight of 178 (anthracene) and 128 molecular weight which express the formation of $[\text{C}_{10}\text{H}_8]$, naphthalene moiety. The whole analysis performed assures a satisfactory synthesis of bis-phenol ligand. Specification of bis-phenol chelating ligand using GC-MS is illustrated in Figure 6.

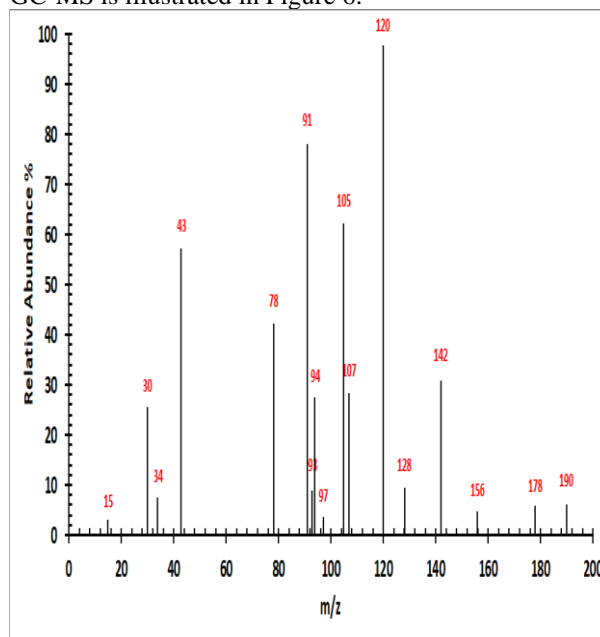


Fig. (6): GC-Mass analysis of hyper cross linkage phosphothiol polymer HCPTP.

^{31}P -NMR analysis

The ^{31}P chemical shift of HCPTP is 28.71 ppm with a single spike that confirms the occurrence of the phosphorylation process and the formation of the HCPTP, Fig. 7.

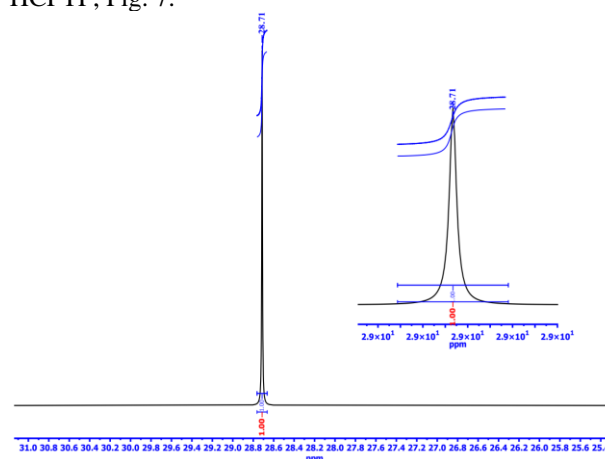


Fig. (7): ^{31}P -NMR analysis of hyper cross linkage phosphothiol polymer HCPTP.

Optimization of Zirconium adsorption using HCPSP

Effect of pH

According to Zr(IV) hydrolysis constants, the distribution of zirconium species in demineralized water at pH values from 0.5 to 4 is presented as Zr^{4+} , $Zr(OH)^{3+}$, $Zr(OH)_2^{2+}$, ZrO_2^{2+} , $Zr(OH)_3^+$, $Zr(OH)_4$. The main species of Zr(IV) in rigorous and moderate acidic media are Zr^{4+} and ZrO_2^{2+} . Meanwhile other species amount increases with increasing of pH value [34]. As shown in figure (8), zirconium adsorption percentage increases with a rise in pH value. At pH below 1, the affinity of HCPSP toward zirconium ions is decreased. This phenomenon is due to the formation of positively charged surface which is resulted in more electrostatic repulsion between zirconium ion and this surface. Furthermore, a weak affinity toward HCPSP in this region can be attributed partly to the competition between the hydronium and zirconium ions [35]. Because of the nature of the acidic functional groups, the acidic functional groups on HCPSP ionize with further rise in pH value and the surface of them becomes more negatively charged which possessed in further electrostatic attraction of zirconium (IV) ions [36]. In the same time, the decrease in the competition between the low concentration of hydronium ions at high pH and zirconium ions can increase the capacity of zirconium adsorption. The obtained results show that the best pH for Zr(IV) adsorption is pH 2 which selected the best pH for this study.

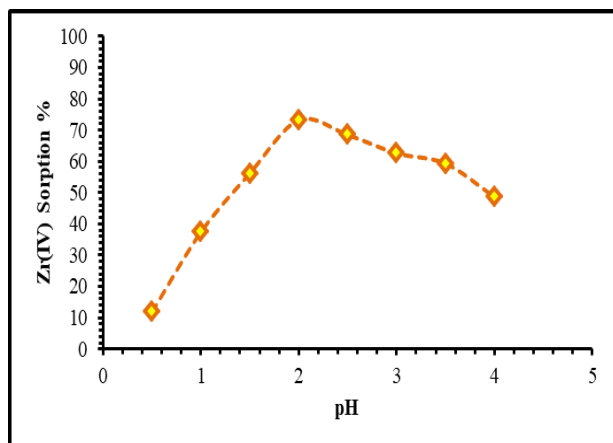


Fig. (8): Effect of pH in the Zr(IV) adsorption % of HCPSP. (Initial conc., 250 ppm/20 ml, time 45 min., 0.1 g weight at room temperature.

Effect of HCPSP dose

The effect of HCPSP dose on Zr(IV) ions adsorption studied and the plotted results indicate that 0.08 g of HCPSP is enough to adsorb fixed amount of Zr(IV) ions. This incident is back to the presence of a lot of unoccupied sites available on the surface of HCPSP but any increase in

the Zr(IV) ions concentration will lead to the difficulty in filling the remaining sites due to the competition effect between Zr(IV) ions. Therefore, 0.08 g will be set for the subsequent experiments at fixed volume of 20 ml uranium pregnant solution (Fig.9)

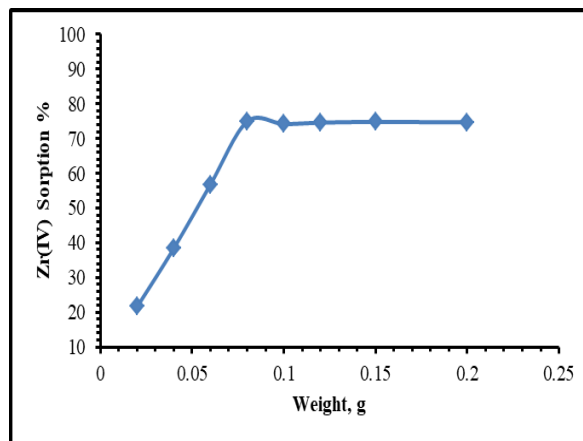


Fig. (9): Effect of HCPSP dose on Zr(IV) ions adsorption.[Zr(IV)]: 250 mg/L, temp. 25°C, contact time: 60 min, 20 mL, pH 2

Effect of Contact Time

The shaking time is an essential factor for estimating the time required for the adsorption process to attain equilibrium. In order to determine the equilibrium time of Zr(IV) on HCPSP, a batch procedure was carried out at different contact times (10-180) min., As shown in Figure 10, the adsorption of Zr(IV) increased when the shaking time increased, and equilibrium is attained after 120 min., the process of zirconium adsorption occurs in two steps; (1) the adsorption of zirconium increases quickly within the first 60 min of contact time and then, (2) the rate of zirconium adsorption process decreases and gradually reaches to the equilibrium time after nearly 2 h of contact time for both initial concentrations. The initial rapid adsorption process could be explained by zirconium adsorption on the external available ion exchange sites of HCPSP and the slow rate of zirconium adsorption may be due to the low diffusion of zirconium ions into the inner cavities and interlayer of HCPSP. Also, it can be seen that the majority of Zr(IV) was adsorbed within the first 120 min. On the other hand, as shown in Fig. 10.

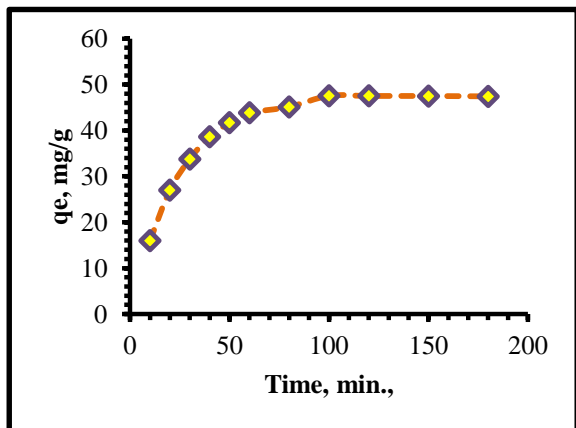


Fig. (10): Effect of contact time on the Zr adsorption percentage by HCPTP, [Zr] = 250 ppm/20ml, pH = 2, T = 25 C, 0.08 g adsorbent, agitation rate = 180 rpm

Sorption kinetic modeling

Adsorption kinetics which indicates the rate of solute uptake on adsorbent, is another important character to determine the potential application of them. The short equilibrium time is the significant parameters for economical adsorption of Zr(IV) and its applications. In order to examine the controlling mechanism of the adsorption process, the pseudo-first-order and the pseudo-second-order rate equation were utilized to analyze the experimental sorption data. The linearized-integral form of the pseudo first-order model is represented by [37]:

$$\log(q_e - q_t) = \log q_e - \left(\frac{k_1}{2.303}\right)t \dots \dots \dots (5)$$

Where k_1 is the rate constant of ions adsorption, q_e and q_t are the amount of Zr(IV) adsorbed (mg/g) at equilibrium and at time t . Values of k_1 was calculated from the slope of the plot of $\log(q_e - q_t)$ against t (Fig. 11) and the values of kinetic parameters for two ions were presented in **Table 3**. The results show that the experimental q_e values are not in agreement with calculated q_e value and the correlation coefficients (R^2) is low. Accordingly, the adsorption of Zr(IV) onto **HCPTP** does not follow this kinetic model.

The linearized-integral form of the pseudo-second-order model is expressed as follows [38]:

$$\frac{t}{qt} = \frac{1}{k_2 q_e^2} + \frac{1}{q_e} t \dots \dots \dots (6)$$

Where k_2 is the pseudo-second-order constant. This rate was determined from the intercept of the plot of t/q_t versus t (Fig. 12). The values of kinetic parameters were listed in **Table 2**. Values of R^2 are > 0.99 and the experimental q_e are in accordance with calculated

q_e illustrate that the adsorption of Zr(IV) onto **HCPTP** fits the pseudo second-order model

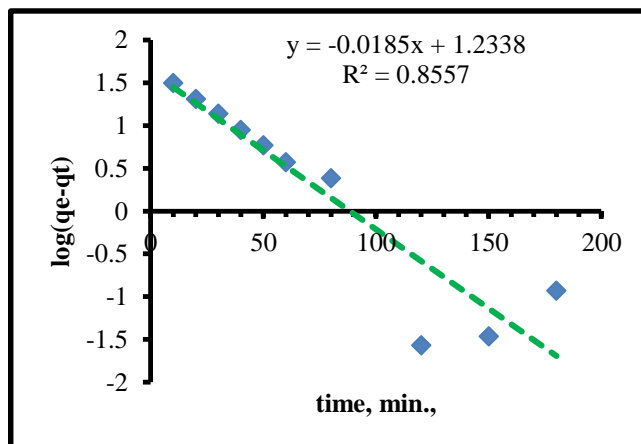


Fig. (11): Pseudo 1st order kinetic model of the adsorption of Zr(IV) on to HCPTP. [[Zr] = 250 ppm/20ml, pH = 2, t = 100 min., T = 25 °C, agitation rate = 180 rpm]

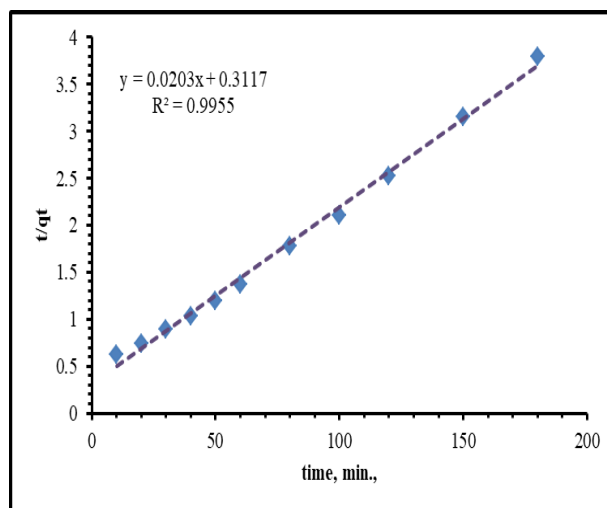


Fig. (12): Pseudo 2nd order kinetic model of the adsorption of Zr(IV) on to HCPTP. [[Zr] = 250 ppm/20ml, pH = 2.5, t = 100 min., T = 25 °C, agitation rate = 180 rpm]

Table (2). Kinetic parameters of Zr(IV) adsorption upon HCPTP

1 st ordered Kinetic			2 nd ordered Kinetic			
K ₁	q _{(max)cal}	R ²	q _{(max)exp}	K ₂	q _{(max)cal}	R ²
0.0426	17.132	0.8557	47.54	0.001322	49.261	0.9955

Effect of initial metal ion concentration

The initial metal ion concentration provides an important driving force to overcome mass transfer resistance between the aqueous and solid phases. The apparent capacity of **HCPSP** for Zr(IV) ions adsorption was investigated for initial concentrations of (100- 1400) (mg/L).

The distribution of Zr(IV) between HCPSP and metal ions in solution, when the adsorption system is at equilibrium, is of valuable importance in clarifying the maximum adsorption capacity of the HCPSP toward the Zr(IV). The analysis of equilibrium sorption data of Zr(IV) is essential to promote equations that represent the results and would be useful for design purposes. Langmuir, and Freundlich models are applied to describe the sorption characteristics of Zr(IV) onto charcoal. [39]

Langmuir isotherm model

Langmuir isotherm is an empirical model assuming that adsorption occurs at a limited number of positions on the adsorbent surface, and the adsorbed layer is one molecule or monolayer adsorption in thickness. The fundamental postulate of this model, the amount of ions adsorbed can be expressed by [40,41]:

$$\frac{C_e}{q_e} = \frac{C_e}{q_m} + \frac{1}{q_m K_l} \dots\dots\dots(5)$$

Where C_e is the equilibrium concentration (mg/L) in the solution, q_e is the amount of ions sorbed on charcoal (mg/g) at equilibrium, Q_{max} is the maximum theoretical monolayer capacity (mg/g), and b is the equilibrium constant of sorption related to the sorption energy. The equilibrium sorption data for Zr(IV) at different temperatures has been correlated with this model, Fig. 9

The figure presentations of (C_e/q_e) versus C_e give straight line for Zr(IV) sorbed onto HCPTP, as presented in **Fig. 13**, with correlation coefficient R^2 less than Freundlich correlation coefficient which suggest that the data is not good represented by Langmuir isotherm. The values of Q_{max} and K_l were calculated from the slop and intercept of the linear plots of C_e/q_e vs. C_e for different temperatures and are listed in **Table 3** with correlation coefficients (R^2). The Langmuir constants Q_{max} and K_l increased with temperature showing that adsorption capacity and equilibrium constant are enhanced at higher temperatures and indicating the endothermic nature of adsorption. The maximum monolayer capacity (Q_{max}) obtained from the Langmuir model was 308 mg/g for Zr(IV) at 25 °C.

The essential features of the Langmuir adsorption isotherm can be expressed in terms of the dimensionless constant (R_l), which is defined using the following relationship:

$$R_l = \frac{1}{1 + K_l C_o} \dots\dots\dots(6)$$

where C_o is the initial total concentration of zirconium, mol l⁻¹; and K_l is the Langmuir isotherm constant. The R_l calculated by the latter equation is 0.41 for zirconium, which indicates that the zirconium adsorption onto the HCPTP is a favorable adsorption process.

Freundlich isotherm model

Freundlich equation is derived to model the multilayer sorption and for the sorption on heterogeneous surfaces. The Freundlich equation agrees well with the Langmuir equation over moderate concentration ranges. The logarithmic form of Freundlich equation may be written as [42-44]

$$\log q_e = \log K_f + \frac{1}{n} \log C_e \dots\dots\dots(6)$$

Where K_f is constant indicative of the relative sorption capacity of charcoal ((mg/g)(L/mg)^{1/n}) and 1/n is the constant indicative of the intensity of the sorption process. The value of 1/n determines the magnitude of adsorption in Freundlich isotherm. If the 1/n value is >1, then the adsorption is not favorable, whereas if the value 1/n <1, then it represents a favorable adsorption. The graphic illustration of log q_e versus log C_e is shown in **Fig. 14** and the numerical values of the constants 1/n and K_f are calculated from the slope and the intercepts, by means of a linear least square fitting method, and also given in **Table 3** The values of R^2 suggest that the data is good represented by Freundlich isotherm and the adsorption of Zr(IV) ions onto the HCP occurs on multilayer sorption on heterogeneous surfaces. Also the value of 1/n is less than 1 which indicate a favorable adsorption of Zr(IV) on HCPTP.

Langmuir isotherm					Freundlich isotherm		
T °C	K _l	q _m	R ²	q _e	K _f	1/n	R ²
25	0.0329	303.03	0.932	307	0.0133	0.5378	0.991
50	0.0279	322.58	0.914	310.5	0.0016	0.7984	0.9904
70	0.0182	333.33	0.956	315	0.00013	0.9822	0.982

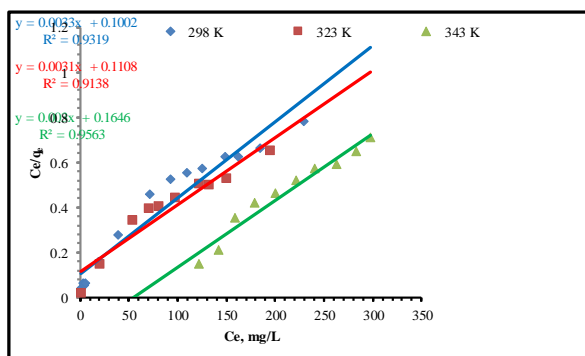


Fig. (13): Langmuir isotherm model of Zr(IV) ions adsorption by HCPTP.

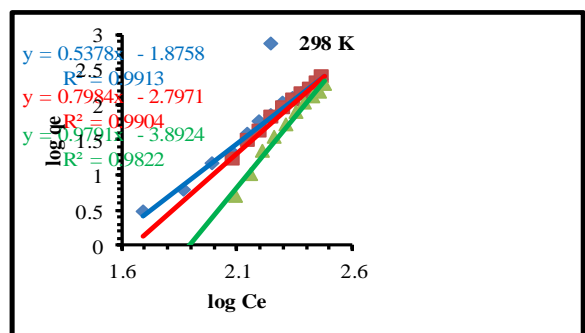


Fig. (14): Freundlich isotherm model of Zr(IV) ions adsorption by HCPTP.

Thermodynamic studies

The Gibbs free energy change, ΔG° , is the fundamental criterion of spontaneity. Reactions occur spontaneously at a given temperature if ΔG° is a negative quantity. The ΔG° of the reaction is given by [45]:

$$\ln K_L = \frac{-\Delta H^\circ}{RT} + \frac{\Delta S^\circ}{R}$$

$$\Delta G^\circ = \Delta H^\circ - T\Delta S^\circ$$

Where T represents the temperature of the adsorbing experiment (K), and R is the gas constant (8.314 J/(mol.K)).

Table (4): Thermodynamic factors for Zr(IV) ions adsorption by HCP at different temperatures.

ΔH° (kJ mol ⁻¹)	ΔS° (J mol ⁻¹ K ⁻¹)	ΔG° (kJ mol ⁻¹)		
		298 K	323 K	343 K
20.702	13.109	-3.886	-4.214	-4.476

The values of ΔH° and ΔS° are tabulated in Table 4. The values of the standard enthalpy changes (ΔH°) are positive and larger than 20 kJ/mol, implying the adsorption of Zr(IV) is endothermic via chemisorption. Furthermore, the positive values of ΔS° show the freedom of Zr(IV) species during the adsorption process and the high degree of randomness at solid-liquid interface during the removal of Zr(IV) species by HCP from the solutions [46]. It is clear to see that the ΔG° values at all sorption temperatures were negative values. This notarize that the sorptive removal process is spontaneous and thermodynamically acceptable. Moreover, the value of ΔG° becomes more negative with the increase of sorption temperature, indicating more efficient sorption of Zr(IV) at high temperature.

Desorption and sorbent recycling (regeneration)

The desorption study has been conducted to regenerate the exhausted adsorbents and restore their character and also to evaluating the possibility to concentrate the target metals, and for evaluating the life cycle of the sorbent through its capacity to be recycled. The regeneration process plays a crucial role in large scale practicing of the feasible treatment process and minimizing the amount of waste (secondary pollutant). In this work, four desorbing agent were used to regenerate the spent adsorbent. The concentration of the released metal ions was determined by ICP-MS. After the elution process the HCPTP was washed repeatedly with distilled water (until pH 7), then it was reloaded with metal ions. The desorption efficiency of the three eluents has been investigated and presented in Fig. 15. the regeneration capacity of HCPSP was more eminent in case of HNO₃, that can easily remove all Zr(IV) ions from the surface of the adsorbent. HNO₃ showed the maximum eluting efficiency of 99.9% after 3 h of incubation. The regenerated HCPTP showed an uptake capacity comparable to that of fresh ones over five cycles.

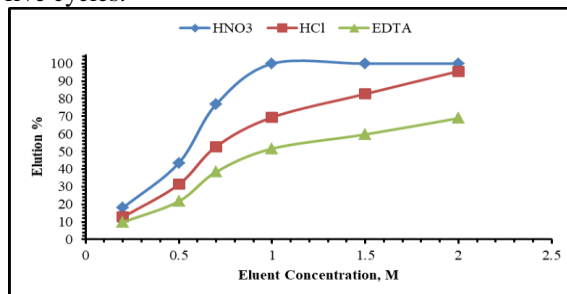


Fig. (15): Effect of different eluting agents on Zr(IV) ions elution from loaded HCP.

The reusability and recycling of HCPTP for the adsorption of Zr(IV) ions.

The recycling of the HCPTP would decrease processing costs and may open the possibility of

recovering the HCPTP after Zr(IV) adsorption. Thus, the ability to recycle the HCPTP is an essential consideration for its practical applications. eight consecutive adsorption-desorption processes investigated the reusability of the HCP. The effects of the number of cycles on the Zr(IV) ions adsorption/desorption capacity are shown in Fig. (16). These results indicate that the HCPTP could be recycled up to four times with more than 97% efficiency, two times over 80%, and two times over 70% while retaining optimal adsorption desorption conditions. The results of this study indicate that the HCPTP could be used as an adsorbent in practical applications for the removal of Zr(IV). Therefore, the HCPTP has potential applications as a high-performance, inexpensive, and recyclable adsorbent for Zr(IV) treatment.

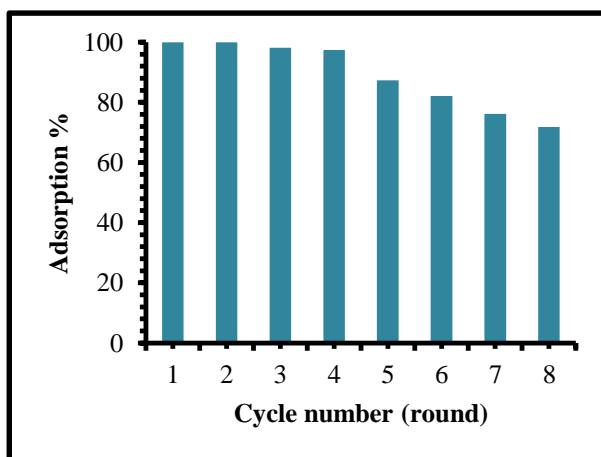
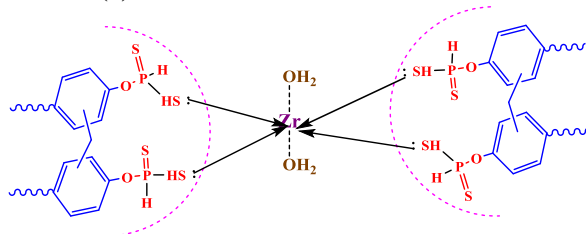


Fig. (16): Recycling of HCPTP for the adsorption of Zr(IV) ions.

Mechanism of interaction between Zr(IV) ions and HCPTP

The interaction between zirconyl ions and HCPSP occurred via chelation coordination mechanism through the sulfur lone pair of electron as outlined in Scheme (2)



Scheme (2): predicted mechanism of interaction of Zr(IV) with HCPTP.

Application on separation of Zr(IV) from Rosetta zircon concentrate

The Selectivity of HCPSP towards Zr(IV) was studied from the synthetic mixture as well as from real matrix samples obtained from the Rosetta zircon concentrate. The chemical analysis of the studied zircon concentrate that separated from black sands is summarized in table (4),

The studied zircon concentrate was separated from black sands. The chemical analysis of studied concentrate is given in Table 4.

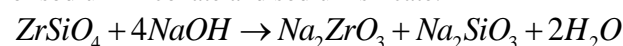
Analyte	Concentration, %
ZrO ₂	65.56
SiO ₂	32.58
HfO ₂	1.32
Fe ₂ O ₃	0.05
TiO ₂	0.05
K ₂ O	0.01
Al ₂ O ₃	0.15

The leaching process was summarized according to the following:

A sample of 50g of Egyptian Rosetta zircon was mixed with 63g of sodium hydroxide pellets and charged to stainless steel crucible. The crucible was then fed to the furnace where the fusion reaction takes

place. The reaction temperature was adjusted at 650 °C for 2h. The fusion product was mixed with (4 times of its weight) distilled water at 60 °C and stirred for 2 hrs to remove sodium silicate solution. The residue (Na₂ZrO₃.H₂SiO₃) was dissolved in concentrated HCl at 90 °C with stirring for 2 hrs then immediately filtrated giving residue which mainly composed of unreacted zircon, TiO₂, Al₂O₃, ThO₂ and H₂SiO₃. The filtrate was crystallized at low temperature giving zirconyl chloride hydrate crystals which then filtrated and dissolved in 1M hydrochloric acid and pH was adjusted to 9 using ammonia solution to precipitate Zr(OH)₄. The obtained zirconium hydroxide was dissolved in certain volume of nitric acid to form of zirconium nitrate solution.

The leaching process of zircon was occurred with caustic soda solution (NaOH) which led to formation of sodium zirconate and sodium silicate.



The obtained sodium silicate was removed through dilution process which led to solubility of sodium silicate while sodium zirconate hydrolyzed onto hydrated zirconia



The obtained zirconium nitrate solution was subjected to adsorption process using HCPTP using the best reached controlling factors for adsorption of Zr(IV), 250 ml leach lacquer with 1 g of HCPTP was stirring for 120 min. with continues stirring at 70 °C, then the HCPTP was then separated by filtration, the obtained HCPTP was treated with 1M HNO₃ to recovering of Zr(IV), after that the solution containing Zr(IV) ions was treated with ammonia solution till the pH reach to 9, to precipitate zirconium as Zr(OH)₄ which filtrated and dried at 60 °C overnight, then burned at 550 °C for 3 hours to form ZrO₂ which used for complete characterization. The obtained product was characterized with XRD, and EDAX, the peak at 2θ = 28.23° in Figure 17a, which is the most intense ZrO₂ diffraction peak of PDF No: 01-089-3045, [47, 48]. The obtained ZrO₂ was confirmed also by recording EDAX spectra Figure 17b. the obtained Emission peaks of O, and Zr were only observed in the EDAX spectrum confirmed the stoichiometry obtained product.

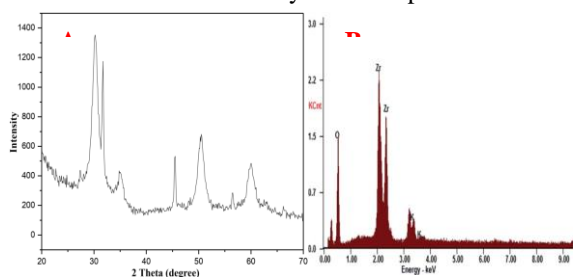


Fig. (17): A. XRD analysis of the obtained ZrO₂, B. EDAX analysis of the obtained ZrO₂

CONCLUSIONS

Hyper cross linkage phosphothiol polymer HCPTP has been synthesized, characterized and used for adsorption of Zr(IV) ions from aqueous solutions. The studied adsorbent HCPTP showed high adsorption capacities towards Zr(IV) ions reached 307 mg/g. The obtained results revealed that the pseudo-second-order sorption is the predominant mechanism. The experimental results from equilibrium experiences were computed by several adsorption isotherm models Langmuir, Freundlich. The results showed that the sorption reaction is more favourable by Freundlich model confirming the multilayer coverage of Zr(IV) onto the HCPTP and indicate the favourability of the chemical adsorption process. The obtained results from batch adsorption studies showed that the optimum adsorbent dose for **HCPTP** was 0.08 g/L from 250 mg/L Zr(IV) ions at pH of 2 and equilibrium time of 100 min., The desorption of Zr(IV) ions from the loaded HCPTP was achieved using 1 M HNO₃.

REFERENCES

- [1] Liu, R., Yang, Z., Chen, S., Yao, J., Mu, Q., Peng, D., Zhao, H., 2019a. Synthesis and facile functionalization of siloxane based hyper-cross-linked porous polymers and their applications in water treatment. *Eur. Polym. J.* 119, 94–101. <https://doi.org/10.1016/j.eurpolymj.2019.07.024>.
- [2] Liu, X., Sun, J., Xu, X., Alsaedi, A., Hayat, T., Li, J., 2019b. Adsorption and desorption of U (VI) on different-size graphene oxide. *Chem. Eng. J.* 360, 941–950. <https://doi.org/10.1016/j.cej.2018.04.050>.
- [3] Wang, X., Liu, F., 2017b. Preparation of phosphorylated graphene oxide and its adsorption performance for U(VI). *Hydrometall. China* 36, 320–327. <https://doi.org/10.13355/j.cnki.sfyj.2017.04.016>.
- [4] Hou, S., Razaque, S., Tan, B., 2019. Effects of synthesis methodology on microporous organic hyper-cross-linked polymers with respect to structural porosity, gas uptake performance and fluorescence properties. *Polym. Chem.* 10, 1299–1311. <https://doi.org/10.1039/c8py01730a>
- [5] Li, B., Gong, R., Wang, W., Huang, X., Zhang, W., Li, H., Hu, C., Tan, B., 2011. A new strategy to microporous polymers: knitting rigid aromatic building blocks by external cross-linker. *Macromolecules* 44, 2410–2414. <https://doi.org/10.1021/ma200630s>
- [6] Xiao, G., Wen, R., Wei, D., Wu, D., 2016. A novel hyper-cross-linked polymeric adsorbent with high microporous surface area and its adsorption to theophylline from aqueous solution. *Microporous Mesoporous Mater.* 228, 168–173. <https://doi.org/10.1016/j.micromeso.2016.03.048>
- [7] Wang, W., Zhou, M., Yuan, D., 2017a. Carbon dioxide capture in amorphous porous organic polymers. *J. Mater. Chem. A* 5, 1334–1347. <https://doi.org/10.1039/C6TA09234A>.
- [8] Li, Q., Zhan, Z., Jin, S., Tan, B., 2017. Wetttable magnetic hypercrosslinked microporous nanoparticle as an efficient adsorbent for water treatment. *Chem. Eng. J.* 326, 109–116. <https://doi.org/10.1016/j.cej.2017.05.049>.
- [9] Tolmacheva, V.V., Yarykin, D.I., Serdiuk, O.N., Apyari, V.V., Dmitrienko, S.G., Zolotov, Y.A., 2018. Adsorption of catecholamines from their aqueous solutions on hypercrosslinked polystyrene. *React. Funct. Polym.* 131, 56–63. <https://doi.org/10.1016/j.reactfunctpolym.2018.07.005>.

- [10] Tan, L., Tan, B., 2017. Hypercrosslinked porous polymer materials: design, synthesis, and applications. *Chem. Soc. Rev.* 46, 3322–3356. <https://doi.org/10.1039/c6cs00851h>.
- [11] Samanta, P., Chandra, P., Ghosh, S.K., 2016. Hydroxy-functionalized hyper-cross-linked ultra-microporous organic polymers for selective CO₂ capture at room temperature. *Beilstein J. Org. Chem.* 12, 1981–1986. <https://doi.org/10.3762/bjoc.12.185>.
- [12] Staudinger, H.; Heuer, W. “Über hochpolymere Verbindungen, 93. Mitteil.: € Über das Zerreißen € der FadenMolekdinger, H., styrols”, *Berichte der deutschen chemischen Gesellschaft (A and B Series)* 1934, 67(7), 1159–1164.
- [13] Davankov, V.; Rogozhin, S.; Tsyurupa, M. “New approach to preparation of uniformLy crosslinked macroreticular polystyrene structures”, *Mezhdunarodnaya Kniga* 1973, 15, 463–465.
- [14] Davankov, V.; Tsyurupa, M.; Ilyin, M.; Pavlova, L. “Hypercross-linked polystyrene and its potentials for liquid chromatography: A mini-review”, *J. Chromatogr. A* 2002, 965(1), 65–73.
- [15] N. Khalid, M. Daud, S. Ahmad, Zirconium decontamination from aqueous media using lateritic minerals, *Radiochim. Acta* 93 (2005) 427–433.
- [16] A.A. Atia, A.M. Donia, H.A. Awaad, Synthesis of magnetic chelating resins functionalized with tetraethylenepentamine for adsorption of molybdate anions from aqueous solutions, *J. Hazard. Mater.* 155 (2008) 100–108.
- [17] Abdel-Rehim, A.M., 2005. A new technique for extracting zirconium form Egyptian zircon concentrate. *Int. J. Miner. Process.* 76, 234–243.
- [18] J.A. Sommers, J.G. Perrine, Method for separation hafnium from zirconium [P]. US200301438, 2003.
- [19] J.S. Liu, H. Chen, Z.L. Guo, Extraction and separation of In (III), Ga(III) and Zn(II) from sulfate solution using extraction resin, *Hydrometallurgy* 82 (2006) 137–143.
- [20] Xiong BK, Wen WG, Yang XM, Li HY, Luo FL, Zhang W, Guo JM (2006) Zirconium and hafnium metallurgy [M]. Metallurgical Industry Press, Beijing.
- [21] Pourreza N, Mouradzadegun A, Mohammadi S (2011) Solid phase extraction of zirconium as arseazo (III) complex on agar and spectrophotometric determination. *J Iran Chem Soc* 8:951–957.
- [22] Zhang A, Wei A, Kumagai M (2003) Properties and mechanism of molybdenum and zirconium adsorption by a macroporous silica-based extraction resin in the MAREC process. *Solvent Extr Ion Exch* 21:591–611.
- [23] Rajmane MM, Sargar BM, Mahamuni SV, Anuse MA (2006) Solvent extraction separation of zirconium (IV) from succinate media with N-n-octylaniline. *J Serbian Chem Soc* 71:223–234.
- [24] Basargin NN, Oskotskaya ER, Simakov PE, Rozovskii YG (2008) Zirconium sorption by chelating polymer sorbents with an o, o0-dihydroxyazo analytical functional group. *Russ J Inorg Chem* 53:1972–1976.
- [25] Bradbrook JS, Lorimer GW, Ridley N (1972) The precipitation of zirconium hydrides in zirconium and zircaloy-2. *J Nucl Mater* 42:142–160.
- [26] Aalahmed, A.H., Briggs, M.E., Cooper, A.I., Adams, D.J., 2019. Post-synthetic fluorination of Scholl-coupled microporous polymers for increased CO₂ uptake and selectivity. *J. Mater. Chem. A* 7, 549–557. <https://doi.org/10.1039/c8ta09359h>.
- [27] Zhang, H., Ruan, Y., Liang, A., Shih, K., Diao, Z., Su, M., Hou, L., Chen, D., Lu, H., Kong, L., 2019a. Carbothermal reduction for preparing nZVI/BC to extract uranium: insight into the iron species dependent uranium adsorption behavior. *J. Clean. Prod.* 239, 117873 <https://doi.org/10.1016/j.jclepro.2019.117873>.
- [28] Zhang, W., Song, Q., Zhang, F., Shu, X., 2019b. Effects of acid treatment and mineral removal on coal chemical composition and wettability. *Coal Convers.* 42, 1–9. <https://doi.org/10.19726/j.cnki.ebcc.201903001>.
- [29] Cai, Y., Wu, C., Liu, Z., Zhang, L., Chen, L., Wang, J., Wang, X., Yang, S., Wang, S., 2017. Fabrication of a phosphorylated graphene oxide–chitosan composite for highly effective and selective capture of U (VI). *Environ. Sci. Nano* 4, 1876–1886. <https://doi.org/10.1039/c7en00412e>.
- [30] Prasun KR, Ashok SR, Pramod KR. Synthesis, characterisation and evaluation of polydithiocarbamate resin supported on macroreticular styrene/divinylbenzene copolymer for the removal of trace and heavy metal ions. *Talanta* 2003;59:239–46.
- [31] Denizli A, Kesenci K, Arica Y, Piskin E. Dithiocarbamate-incorporated monosize polystyrene microspheres for selective removal of mercury ions. *React Funct Polym* 2000;44:235–43.
- [32] Costa PA, Teixeira VG. Influence of the matrix porosity on the synthesis and adsorption behavior of dithiocarbamate styrenic resins toward zinc(II) and cadmium(II) Ions. *J Appl Polymer Sci* 2010;116:3070–8.
- [33] Samanta, P., Chandra, P., Ghosh, S.K., 2016. Hydroxy-functionalized hyper-cross-linked ultra-microporous organic polymers for selective CO₂

- capture at room temperature. *Beilstein J. Org. Chem.* 12, 1981–1986. <https://doi.org/10.3762/bjoc.12.185>.
- [34] Pourbaix M (1974) Atlas of electrochemical equilibria in aqueous solutions. The University of Michigan: National Association of Corrosion Engineers, Houston.
- [35] Rao GP, Lu C, Su F (2007) Sorption of divalent metal ions from aqueous solution by carbon nanotubes: a review. *Sep Purif Technol* 58:224–231.
- [36] Yavari R, Huang YD, Mostofizadeh A (2012) Sorption of strontium ions from aqueous solutions by oxidized multiwall carbon nanotubes. *J Radioanal Nucl Chem* 285:703–710
- [37] Y.L. Liu, W.H. Chen and Y.H. Chang, *Carbohydr. Polym.* 76, 232 (2009). doi:10.1016/j.carbpol.2008.10.021.
- [38] H.L. Wang, J.L. Chen and Q.-X. Zhang, Adsorption of an Amphoteric Aromatic Compound (PAminobenzoic Acid) onto Different Polymeric Adsorbents. *Adsorpt. Sci. Technol.* 24, 17 (2006) doi:10.1260/026361706778062540.
- [39] R. Donat, K.E. Erden, Adsorption of U(VI) ions from aqueous solutions by activated carbon prepared from Antep pistachio (*Pistacia vera* L.) shells, *Radiochim. Acta* 105 (2017) 359–367.
- [40] I. Langmuir, The constitution and fundamental properties of solids and liquids, *J. Am. Chem. Soc.* 38 (1916) 2221–2295.
- [41] M.M. Hamed, M. Holiel, Y.F. El-Aryan, Removal of selenium and iodine radionuclides from waste solutions using synthetic inorganic ion exchanger, *J. Mol. Liq.* 242 (2017) 722–731.
- [42] H.M.F. Freundlich, Over the adsorption in solution, *J. Phys. Chem.* 57 (1906) 385.
- [43] L. Peng, W. Hanyu, Y. Ni, Y. Zhuoxin, P. Duoqiang, W. Wangsuo, β -Zeolite modified by ethylenediamine for sorption of Th(IV), *Radiochim. Acta* 105 (2017) 463–471.
- [44] A.A. Zaki, M.I. Ahmad, K.M. Abd El-Rahman, Sorption characteristics of a landfill clay soil as a retardation barrier of some heavy metals, *Appl. Clay Sci.* 35 (2017) 150–167
- [45] Gado M., Atia B., Morcy A. The role of graphene oxide anchored 1-amino-2-naphthol-4-sulphonic acid on the adsorption of uranyl ions from aqueous solution: kinetic and thermodynamic features. *Int. J. Environ. Anal. Chem.* 2019, 99, 996–1015.
- [46] Zeng ZH, Wei YQ, Shen L and Hua DB, Cationically charged poly(amidoxime)-grafted polypropylene nonwoven fabric for potential uranium extraction from seawater. *Ind Eng Chem Res* 54:8699–8705 (2015).
- [47] B. Tyagi, K. Sidhpuria, B. Shaik, R.V. Jasra, “Synthesis of nanocrystalline zirconia using sol-gel and precipitation techniques,” *Ind. Eng. Chem. Res.* Vol. 45, pp. 8643–8650, 2006.
- [48] S. Vivekanandhan, M. Venkateswarlu, H.R. Rawls, N. Satyanarayana, “Acrylamide assisted polymeric citrate route for the synthesis of nanocrystalline ZrO₂ powder,” *Materials Chemistry and Physics*, vol. 120, pp. 148–154, 201.